

A novel method for the measurement of liquid film thickness during fuel spray impingement on surfaces

S. Henkel,¹ F. Beyrau,² Y. Hardalupas,^{1,*} and A.M.K.P. Taylor¹

¹ Department of Mechanical Engineering, Imperial College London, SW7 2AZ, London, UK

² Lehrstuhl für Technische Thermodynamik, Otto-von-Guericke-Universität Magdeburg, 39106 Magdeburg, Germany

* y.hardalupas@imperial.ac.uk

Abstract: This paper describes the development and application of a novel optical technique for the measurement of liquid film thickness formed on surfaces during the impingement of automotive fuel sprays. The technique makes use of the change of the light scattering characteristics of a metal surface with known roughness, when liquid is deposited. Important advantages of the technique over previously established methods are the ability to measure the time-dependent spatial distribution of the liquid film without a need to add a fluorescent tracer to the liquid, while the measurement principle is not influenced by changes of the pressure and temperature of the liquid or the surrounding gas phase. Also, there is no need for non-fluorescing surrogate fuels. However, an *in-situ* calibration of the dependence of signal intensity on liquid film thickness is required. The developed method can be applied to measure the time-dependent and two-dimensional distribution of the liquid fuel film thickness on the piston or the liner of gasoline direct injection (GDI) engines.

The applicability of this technique was evaluated with impinging sprays of several linear alkanes and alcohols with different thermo-physical properties. The surface temperature of the impingement plate was controlled to simulate the range of piston surface temperatures inside a GDI engine. Two sets of liquid film thickness measurements were obtained. During the first set, the surface temperature of the plate was kept constant, while the spray of different fuels interacted with the surface. In the second set, the plate temperature was adjusted to match the boiling temperature of each fuel. In this way, the influence of the surface temperature on the liquid film created by the spray of different fuels and their evaporation characteristics could be demonstrated.

©2016 Optical Society of America

OCIS codes: (000.2170) Equipment and techniques; (120.4820) Optical systems; (240.0310) Thin films; (240.5770) Roughness; (290.5880) Scattering, rough surfaces; (310.6870) Thin films, other properties

References and links

1. R. van Basshuysen and U. Spicher, *Gasoline Engine with Direct Injection: Processes, Systems, Development, Potential*. Wiesbaden: Springer Verlag, 2009.
2. M. C. Drake and T. D. Fansler, "Piston Fuel Films as a Source of Smoke and Hydrocarbon Emissions from a Wall-Controlled Spark-Ignited Direct-Injection Engine," SAE Tech. Pap. Ser., (2003-01-0547), (2003).
3. M. C. Drake and D. C. Haworth, "Advanced gasoline engine development using optical diagnostics and numerical modeling," Proc. Combust. Inst., **31**(1), 99-124 (2007).
4. X. He, M. A. Ratcliff, and B. T. Zig, "Effects of Gasoline Direct Injection Engine Operating Parameters on Particle Number Emissions," Energy & Fuels, **26**(4), 2014-2027 (2012).
5. S. Malaguti and S. Fontanesi, "CFD Investigation of Fuel Film Formation Within a GDI Engine Under Cold Start Cranking Operation," Proc. 2009 Spring Tech. Conf. ASME Int. Combust. Engine Div., 555-562

- (2009).
6. F. F. Zhao, D. L. Harrington, and M. C. Lai, *Automotive Gasoline Direct-Injection Engines*. Oxford: Society of Automotive Engineers, 2002.
 7. B. D. Stojkovic, T. D. Fansler, M. C. Drake, and V. Sick, "High-speed imaging of OH* and soot temperature and concentration in a stratified-charge direct-injection gasoline engine," *Proc. Combust. Inst.*, **30**(2), 2657–2665 (2005).
 8. M. M. Maricq, "Chemical characterization of particulate emissions from diesel engines: A review," *J. Aerosol Sci.*, **38**(11), 1079–1118 (2007).
 9. E. Hecht, *Optics*. San Francisco: Addison-Wesley Longman, Incorporated, 2002.
 10. T. Ohyama, K. Endoh, A. Mikami, and Y. H. Mori, "Optical interferometry for measuring instantaneous thickness of transparent solid and liquid films," *Rev. Sci. Instrum.*, **59**(9), 2018–2022 (1988).
 11. S.-W. Kim and G.-H. Kim, "Thickness-Profile Measurement of Transparent Thin-Film Layers by White-Light Scanning Interferometry," *Appl. Opt.*, **38**(28), 5968–5973 (1999).
 12. N. Borgetto, C. Galizzi, F. André, and D. Escudié, "A thickness measurement technique based on low-coherence interferometry applied to a liquid film with thermal gradient," *Exp. Therm. Fluid Sci.*, **34**(8), 1242–1246 (2010).
 13. F. Gao, H. Muhamedsalih, and X. Jiang, "Surface and thickness measurement of a transparent film using wavelength scanning interferometry," *Opt. Express*, **20**(19), 21450–6 (2012).
 14. X. Jiang, K. Wang, F. Gao, and H. Muhamedsalih, "Fast surface measurement using wavelength scanning interferometry with compensation of environmental noise," *Appl. Opt.*, **49**(15), 2903–2909 (2010).
 15. S. K. Debnath, M. P. Kothiyal, J. Schmit, and P. Hariharan, "Spectrally resolved phase-shifting interferometry of transparent thin films: sensitivity of thickness measurements," *Appl. Opt.*, **45**(34), 8636–40 (2006).
 16. X. S. Wang and H. H. Qiu, "Fringe probing of liquid film thickness of a plug bubble in a micropipe," *Meas. Sci. Technol.*, **16**(2), 594–600 (2005).
 17. A. Kariyasaki, Y. Yamasaki, M. Kagawa, T. Nagashima, A. Ousaka, and S. Morooka, "Measurement of Liquid Film Thickness by a Fringe Method," *Heat Transf. Eng.*, **30**(1–2), 28–36 (2009).
 18. M. Kuhner and E. Sackmann, "Ultrathin hydrated dextran films grafted on glass: Preparation and characterization of structural, viscous, and elastic properties by quantitative microinterferometry," *Langmuir*, **12**(20), 4866–4876 (1996).
 19. G. Wiegand, K. R. Neumaier, and E. Sackmann, "Microinterferometry: Three-Dimensional Reconstruction of Surface Microtopography for Thin-Film and Wetting Studies by Reflection Interference Contrast Microscopy (RICM)," *Appl. Opt.*, **37**(29), 6892–6905 (1998).
 20. I. B. Ozdemir and J. H. Whitelaw, "An Optical Method for the Measurement of Unsteady Film Thickness," *Exp. Fluids*, **13**(5), 321–331 (1992).
 21. C. Schulz and V. Sick, "Tracer-LIF diagnostics: quantitative measurement of fuel concentration, temperature and fuel/air ratio in practical combustion systems," *Prog. Energy Combust. Sci.*, **31**(1), 75–121 (Jan. 2005).
 22. A. C. Eckbreth, *Laser Diagnostics for Combustion Temperature and Species*. Amsterdam: Gordon and Breach Publishers, 1996.
 23. M. Alonso, P. J. Kay, P. J. Bowen, R. Gilchrist, and S. Sapsford, "A laser induced fluorescence technique for quantifying transient liquid fuel films utilising total internal reflection," *Exp. Fluids*, **48**(1), 133–142 (2010).
 24. T. Fujikawa, Y. Hattori, M. Koike, K. Akihama, T. Kobayashi, and S. Matsushita, "Quantitative 2-D fuel distribution measurements in a direct-injection gasoline engine using laser-induced fluorescence technique," *JSME Int. J. Ser. B-Fluids Therm. Eng.*, **42**(4), 760–767 (1999).
 25. Y. Cheng, K. Deng, and T. Li, "Measurement and simulation of wall-wetted fuel film thickness," *Int. J. Therm. Sci.*, **49**(4), 733–739 (2010).
 26. F. Schulz, J. Schmidt, and F. Beyrau, "Development of a sensitive Experimental Set-up for LIF Fuel Wall Film Measurements in a Pressure Vessel," *Accept. Publ. Exp. Fluids*, (2015).
 27. I. Duewel, J. Schorr, P. Peuser, P. Zeller, J. Wolfrum, and C. Schulz, "Spray diagnostics using an all-solid-state Nd:YAlO₃ laser and fluorescence tracers in commercial gasoline and diesel fuels," *Appl. Phys. B*, **79**(2), 249–254 (2004).
 28. R. Domann and Y. Hardalupas, "Spatial distribution of fluorescence intensity within large droplets and its dependence on dye concentration," *Appl. Opt.*, **40**(21), 3586–3597 (2001).
 29. M. Davy, P. Williams, D. Han, and R. Steeper, "Evaporation characteristics of the 3-pentanone-isooctane binary system," *Exp. Fluids*, **35**(1), 92–99 (2003).
 30. D. Greszik, H. Yang, T. Dreier, and C. Schulz, "Laser-based diagnostics for the measurement of liquid water film thickness," *Appl. Opt.*, **50**(4), A60–A67 (2011).
 31. I. K. Kabardin, V. G. Meledin, I. a. Eliseev, and V. V. Rakhmanov, "Optical measurement of instantaneous liquid film thickness based on total internal reflection," *J. Eng. Thermophys.*, **20**(4), 407–415 (2011).
 32. C. H. Hidrovo and D. P. Hart, "Emission reabsorption laser induced fluorescence (ERLIF) film thickness measurement," *Meas. Sci. Technol.*, **12**(4), 467–477 (2001).
 33. A. A. Mouza, N. A. Vlachos, S. V. Paras, and A. J. Karabelas, "Measurement of liquid film thickness using a laser light absorption method," *Exp. Fluids*, **28**(4), 355–359 (2000).
 34. B. Commoner and D. Lipkin, "The Application of the Beer-Lambert Law to Optically Anisotropic Systems," *Science* (80-.), **110**(2845), 41–43 (1949).
 35. H. Yang, D. Greszik, T. Dreier, and C. Schulz, "Simultaneous measurement of liquid water film thickness

- and vapor temperature using near-infrared tunable diode laser spectroscopy,” *Appl. Phys. B*, **99**(3), 385–390 (2010).
36. G. M. Hale and M. R. Query, “Optical Constants of Water in the 200-nm to 200-micrometer Wavelength Region,” *Appl. Opt.*, **12**(3), 555–563 (1973).
 37. M. C. Fansler, T.D., Drake, “Optical Diagnostics Applied to Spark-Ignited Direct-Injection Engine Development,” 5. Int. Symp. fuer Verbrennungsdiagnostik, Baden-bad., (2002).
 38. M. E. Drake, M.C. , Fansler, T.D. , and Rosalik, “Quantitative high-speed imaging of piston fuel films in direct-injection engines using a refractive-index- matching technique,” ILASS-02 – 15th Annu. Conf. Liq. At. Spray Syst. Madison, WI, (2002).
 39. B. Yang and J. Ghandhi, “Measurement of Diesel Spray Impingement and Fuel Film Characteristics Using Refractive Index Matching Method,” SAE Tech. Pap. Ser., (2007–01–0485), (2007).
 40. D. Maligne and G. Bruneaux, “Time-Resolved Fuel Film Thickness Measurement for Direct Injection SI Engines Using Refractive Index Matching,” SAE Tech. Pap. Ser., (2011–01–1215), (2011).
 41. Q. Lu, N. V. Suryanarayana, and C. Christododoulou, “Film Thickness Measurement with an Ultrasonic Transducer,” *Exp. Therm. Fluid Sci.*, **7**(4), 354–361 (1993).
 42. P. C. Pedersen, Z. Cakareski, and J. C. Hermanson, “Ultrasonic monitoring of film condensation for applications in reduced gravity,” *Ultrasonics*, **38**(1–8), 486–490 (2000).
 43. M. W. E. Coney, “The theory and application of conductance probes for the measurement of liquid film thickness in two-phase flow,” *J. Phys. E.*, **6**(9), 903 (1973).
 44. T. Fukano, “Measurement of time varying thickness of liquid film flowing with high speed gas flow by a constant electric current method (CECM),” *Nucl. Eng. Des.*, **184**(2–3), 363–377 (1998).
 45. P. Selegim and E. Hervieu, “Direct imaging of two-phase flows by electrical impedance measurements,” *Meas. Sci. Technol.*, **9**(9), 1492–1500 (1998).
 46. M. R. Ozgu, J. C. Chen, and N. Eberhardt, “A capacitance method for measurement of film thickness in two-phase flow,” *Rev. Sci. Instrum.*, **44**(12), 1714–1716 (1973).
 47. J. F. Klausner, L. Z. Zeng, and D. M. Bernhard, “Development of a film thickness probe using capacitance for asymmetrical two-phase flow with heat addition,” *Rev. Sci. Instrum.*, **63**(5), 3147–3152 (1992).
 48. M. Raffel, C. E. Willert, S. T. Wereley, and J. Kompenhans, *Particle Image Velocimetry: A Practical Guide*. Heidelberg: Springer, 2007.
 49. J. Weickert, “A review of nonlinear diffusion filtering,” in *Scale-Space Theory in Computer Vision SE - 1*, **1252**, B. Haar Romeny, L. Florack, J. Koenderink, and M. Viergever, Eds. Springer Berlin Heidelberg, 1–28 1997.
 50. J. Weickert, B. M. T. H. Romeny, and M. A. Viergever, “Efficient and reliable schemes for nonlinear diffusion filtering,” *Image Process. IEEE Trans.*, **7**(3), 398–410 (1998).
 51. S. Pfadler, F. Beyrau, and A. Leipertz, “Flame front detection and characterization using conditioned particle image velocimetry (CPIV),” *Opt. Express*, **15**(23), 15444–15456 (2007).
 52. “NIST Chemisrty Webbook,” *NIST Standard Reference Database Number 69*. [Online]. Available: <http://webbook.nist.gov/chemistry/>.
-

1. Introduction

Wall wetting is a widely observed phenomenon in many engineering applications. This process describes the formation of a liquid layer on a solid surface. In applications where a liquid spray is injected into a chamber this is usually an unwanted problem. One particular example of this process is the piston wetting during the fuel injection process [1] inside a gasoline direct injection engine. In this context, previous experiments showed a connection between particulate emissions at the exhaust and the formation of a fuel liquid film on the piston. During the combustion process, wall wetting can lead to pool fires linked with rich diffusion flames on top of the liquid deposit [2–7]. This can contribute to unwanted increase in pollutant formation and an increase of unburned hydrocarbons due to insufficient mixing between air and fuel [2]. It becomes more and more important for car manufacturers to minimize these effects, since governmental regulations demand a low threshold of emissions from modern cars [8]. As such, it is of great interest to get a better understanding of the physical process involved in liquid fuel deposition and subsequent evaporation and the influence of the fuel characteristics and surface temperatures.

One family of techniques for liquid film thickness measurements is based on interferometry. This principle links the interference of two or more scattered light waves from the liquid film to form a spatial interference fringe pattern [9]. This interference pattern can yield information about the thickness of transparent liquid films [10, 11]. There are several different versions of interferometry used to investigate thin liquid films. Borgetto *et al.* [12]

used low-coherence interferometry (LCI) to measure liquid film thickness of linear alkanes. In their case, a super luminescent LED (light emitting diode) was used as a light source to illuminate the film and create interference patterns. From the spacing between individual maxima in the interferogram, it was possible to measure the film thickness. Gao *et al.* [13] used wavelength scanning interferometry to investigate transparent films. Combining a white light interferometer with a near-infrared super luminescent light-emitting diode interferometer, it was possible to measure the liquid film thickness, while compensating for environmental noise and vibrations at the same time [13, 14]. Debnath *et al.* [15] used spectrally resolved phase-shifting interferometry to investigate thin transparent films illuminated by a white light source. They were able to measure the thickness of a thin transparent film on a reflecting substrate by analysing the phase shift in spectrally resolved interferograms. All presented methods of interferometry have a common limitation that they can only measure along a line. Also, the temporal resolution of the technique is somewhat limited. This means that, for investigations of highly unsteady liquid deposits, these techniques might not be reliable.

Similar to the interferometry method is the so-called fringe method. This technique is often used to measure the thickness of liquid films in capillaries or investigate two phase flows inside small diameter tubes [16]. Kariyasaki *et al.* [17] showed that this technique can also be used to measure the film thickness of thin transparent films on top of a solid surface. By using parallel illumination of the liquid film with a coherent light source at a fixed angle, it is possible to create fringe patterns [18, 19] due to the fact that the liquid film is not perfectly uniform across the surface. Therefore, the parallel light gets refracted and reflected at different locations of the film. The reflected and refracted light can interfere and create a spatial fringe pattern that changes with the local film thickness. Since the fringe pattern is formed at the surface of the liquid film, precise focusing of the optical system is necessary. Kariyasaki *et al.* [17] used a microscope with a CCD camera to generate and record the fringe patterns. They presented thickness profiles across the spatial distribution of a liquid film. In another set of experiments, they showed that it is possible to track and quantify an evaporating hexane film over time by using shorter exposure times and higher recording frequencies. The advantage of the fringe method is its high sensitivity on the local film thickness, even in multi-phase flows [17]. With the presented realisation of this technique, however, it is only possible to measure along a line and not in two dimensions. Furthermore, the temporal resolution illustrated with a volatile liquid at room temperature might not be sufficient at higher temperatures, especially if the boiling point of the liquid is exceeded. Additionally, the rather complex optical alignment might limit the *in-situ* application of this technique to an injection chamber or pressure vessel, where the angle of illumination is fixed and the optical distance to the specimen may be large.

Another technique based on the fringe pattern formation was used by Ozdemir and Whitelaw [20]. They derived an analytical correlation between the interferometric fringe pattern and the thickness of an unsteady liquid film. Solving for the optical transformation function of their optical setup, the intensity fluctuations created by the fringes could be linked to the film thickness without the need for a separate calibration. Using a photodiode to detect the signal, they were able to achieve a high temporal resolution. However, the recordings only yielded time-dependent liquid film thickness measurements at a point, similar to the techniques discussed earlier.

Probably the most commonly applied technique to investigate liquid deposits on solid surfaces is based on Laser Induced Fluorescence (LIF) [21]. Fluorescence describes the spontaneous emission of radiation from an electronically excited molecule. In the case of LIF, this excitation is generated by the laser light source [22]. This method requires a fluorescent proxies to be present in the liquid. This can be either one of the components of the liquid itself or a fluorescent dye added to the liquid. In both cases, a laser is used to excite the tracer molecules, which then emit a fluorescence signal. If the laser intensity and the concentration of the tracer in the liquid are constant, it is possible to relate the recorded fluorescent intensity signal to the amount of liquid on the surface [21]. Also, with the use of appropriate optical

components, it is possible to illuminate the entire liquid film. In this way, the emitted fluorescent intensity from the entire area of the liquid deposit can be captured, usually with a CCD camera, which includes information on the local film thickness. With such an optical setup it is possible to obtain spatially and temporally resolved information. However, selecting the tracer can be challenging for this kind of application [23]. Ideally, the tracer should yield a strong fluorescent intensity signal, while remaining proportional to the concentration of the tracer and insensitive to changes, such as pressure and temperature. Also, the tracer should show the same physical behaviour as the investigated fuel. This means properties like evaporation rate, diffusivity, convection, surface tension and viscosity should be the same. In practical applications it is usually not possible to find a tracer which meets all of these requirements [23]. For investigations that involve multi-component liquid fuels, like gasoline, it is common to replace the original fuel with a mixture of a fluorescent tracer and non-fluorescing fuel substitute. This can be 3-pentanone which is excitable with a UV laser and iso-octane as a non-fluorescing surrogate fuel [23–26]. However, the evaporation behaviour of this fuel is, depending on the conditions, certainly not directly comparable to that of real gasoline. In a scenario where a set of real gasoline blends need to be investigated, such substitution of a fuel component is not an option. Alternatively, it is possible to add a strongly fluorescent dye which acts as the tracer substance to the real fuel. These dyes have a very high fluorescence yield, which means only small amounts need to be added to the fuel [27]. This way the physical properties of the liquid remain largely unchanged, usually without any effect on the measurement. However, care should be taken to ensure that the absorption of the incident light within thick liquid films does not lead to a non-linear dependence of the fluorescent intensity on the fluorescent dye concentration [28]. The downside of this concept is that they do not co-evaporate with the liquid of interest [29] and the dye concentration changes over time. This means it is not possible to obtain a reliable time-dependent signal of the evaporating liquid deposit. Consequently, only films which are not significantly affected by evaporation can be investigated in order to minimize this error. Both approaches, with an added dye or a liquid tracer, have the disadvantage that by illuminating the liquid film it is very likely that the region above the liquid film is also illuminated. This means that the fluorescent intensity signal not only corresponds to the actual liquid film but also to the areas above it. Alonso *et al.* [23], Greszik *et al.* [30] and Kabadin *et al.* [31] developed a method to overcome this issue. By coupling the light source into the glass plate where the liquid deposit is formed on, it is possible to achieve total internal reflection between the glass plate and the surrounding air. Hence, the light escapes from the glass plate only at those positions where it is covered by a liquid layer. To further improve the LIF technique, Hidrovo *et al.* [32] presented a method called reemission reabsorption laser induced fluorescence. Essentially, the physical fundamentals are based on LIF, however, it uses emission and subsequent reabsorption of two different dyes instead of pure fluorescence of a single tracer. The absorption and emission spectra were selected in a way that the fluorescent wavelength of the first dye overlapped with the absorption spectrum of the second. The latter then fluoresces at a third wavelength. By calculating the ratio between the two fluorescence signals, it was possible to very accurately determine the actual film thickness, because effects such as reflection and changes in illumination intensity were cancelled out. The detection of two wavelengths, however, makes the optical setup more complex compared to ordinary LIF. Hidrovo *et al.* [24] used two CCD cameras equipped with optical filters and mounted on the same lens with an optical-path-splitting module. In this way, it was possible to ensure good overlap between the two images and achieve very high accuracy during their measurements. Furthermore, using the fluorescence intensity ratio makes the calibration independent of the optical characteristics of a particular setup as they are cancelled out by the normalisation. The downside of the reabsorption method is the limited range of film thicknesses it can be applied to. The main factor is the necessity of an optically thick medium with enough reabsorption to be able to accurately quantify the thickness. In combination with the non-evaporative behaviour

of the dyes, this technique might not be reliable enough for investigations of evaporating fuel deposits.

An additional laser based technique to measure liquid film thicknesses is the laser light absorption method. Mouza *et al.* [33] used the absorption of light from a diode laser passing through a thin liquid film which contained a dye. Using the law of Beer and Lambert, it is possible to determine the film thickness by measuring the absorption ratio in a calibrated system [34]. The light source used in these experiments was a low power diode laser. The signal was recorded with a silicon photodiode at a fixed distance from the light source. This setup yielded zero-dimensional measurements. In the case of a steady film, it would be possible to move the laser and detector along a line across the film. Consequently, spatial information of the liquid deposit would be available. Generally, this particular method is very similar to the dye based LIF technique, only the physical principle is different. This means that the advantages and disadvantages also apply here. Dye based absorption measurements yield a good signal with very little tracer concentration. The dye used by Mouza *et al.* [33] was methylene blue, which does not co-evaporate and hence is only suitable for non-evaporating deposits or measurements with no temporal resolution. Yang *et al.* [35] used a near-infrared (NIR) diode laser to measure the thickness of liquid water films. In these experiments, the addition of a tracer is not necessary, since liquid water shows broad band absorption for infrared light [36]. In order to further separate the absorption signal from any background noise, they used two diode lasers of different IR wavelength, both being absorbed by water. Since the absorption spectrum of water changes with temperature, it was also possible to obtain temperature information. A later work by Greszik *et al.* [30] compared this method to LIF and spontaneous Raman scattering. As a result they were able to show that both the spontaneous Raman and the NIR based techniques can capture the evaporation behaviour of water films very well. However, not all liquids, such as gasoline, absorb at the NIR range. This would mean that in such applications a chemical tracer would be necessary. This fact causes the same dilemma for this type of investigations as the LIF based methods.

A rather novel optical technique used to investigate liquid deposits called Refractive Index Matching (RIM) was developed by Drake *et al.* [37] and first presented in 2002 [2, 37, 38]. It was used to quantitatively analyze liquid deposit formation on the glass piston surface of an optically accessible gasoline direct injection engine. Due to the temperature changes during the cycles of the engine, the use of a LIF based method was not favored, because of the temperature dependence of the fluorescent signal. Refractive Index Matching provides quantitative information about the fuel deposit with large temporal and spatial resolution while remaining insensitive to temperature and pressure variations. Also, this method works for single and multi-component fuels [2]. The physical basis of RIM is that light scattering behavior of a rough glass plate is changing with the thickness of a liquid deposit on top of it. The refractive index of the liquid and the glass are approximately matching. The observed change can then be correlated to the thickness of the liquid by using an appropriate calibration. Yang *et al.* [39] were using RIM to investigate impinging Diesel sprays in a heated test chamber and the effect of changing air temperature on the deposit. Maligne *et al.* [40] used the Refractive Index Matching technique to conduct time resolved measurements of fuel deposit formed by a gasoline spray impinging on a glass plate. Overall RIM has the advantage of making a tracer addition unnecessary and being independent of temperature and pressure changes. However, the use of a glass piston instead of the actual metal piston in an engine might change the heat flux into the liquid deposit and therefore its evaporation behaviour. This could hinder investigations focusing on exactly this process.

Apart from optical methods presented here, there are also acoustic techniques used to investigate liquid films. Commonly, these are utilising ultrasonic waves, which are attenuated and reflected due to discontinuities created by liquid/gas interfaces. The application of different iterations of acoustic techniques can be found in [41] and [42].

As a final class, electrical techniques shall be mentioned. These are split into conductance-based and capacitance-based methods. The former uses electrodes to generate an electrical potential difference. The resulting current between the electrodes can be related to the liquid film thickness. Applications are presented in [43–45]. The capacitance method uses two parallel metal plates to form a capacitor by applying electrical current to them. The capacitance is then changed if a liquid film is present. This change can be linked to the thickness of the deposit. Further details can be found in [46] and [47].

In the presented study a new technique was developed to investigate liquid deposits created by impinging sprays, similar to those found in direct injection engines. Similar to RIM, the technique relies on the change of the light scattering behaviour of a rough solid surface, once liquid is applied. In this case, however, a treated metal plate was used instead of a glass piston. With the use of a rough metal surface, it was possible to resemble the conditions found inside the cylinder of an engine more closely, compared to other techniques. The temperature of the metal surface was adjustable, which allowed insight into the effect of the surface temperature on the liquid deposit.

2. Experimental setup

The experimental setup presented in Fig. 1 comprises of an injection chamber with the injector, an impingement plate and a fuel preparation section. The injection chamber consisted of a cubical frame with a length of 300 mm. It was mounted on a metal base plate elevated with feet, allowing for the connection of a vapour extraction system. The sides of the chamber could be closed with polycarbonate windows and sealed off with rubber gaskets. Also the contact area between the frame and the base plate was sealed with rubber foaming. In this way, stable ambient conditions could be achieved and maintained. The rear of the chamber was closed with an aluminium plate that formed the support of the impingement plate. The hollow impingement plate was mounted with aluminium brackets and could be purged with conditioned silicone oil (Rhodorsil 47V100, Bentley Advanced Materials). The plate was connected to a heat exchanger (Julabo ME-12, Julabo UK LTD), which could control the plate temperature automatically with the help of a temperature sensor inside the plate. Furthermore, the surface temperature was checked with a k-type thermocouple. An additional air heater (LHS 21L System, Leister AG) could be used to stabilise the ambient temperature inside the injection chamber.

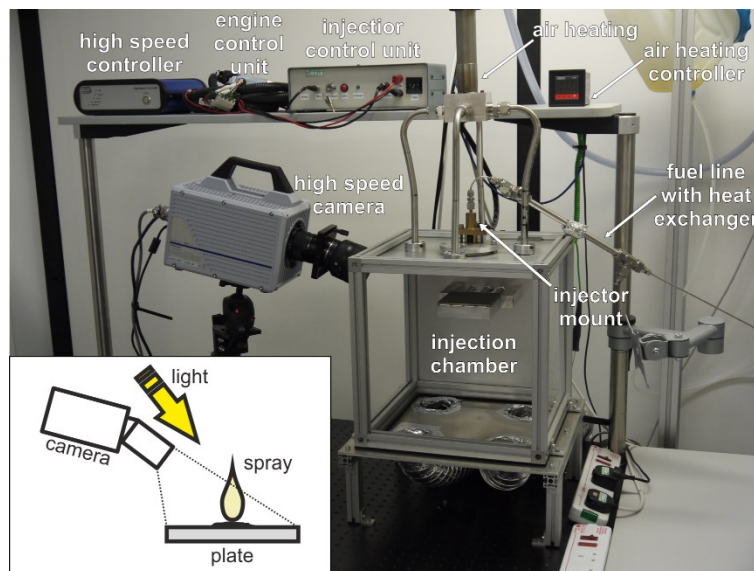


Fig. 1. Overview of the experimental setup with a schematic of the camera and light source arrangement.

The top was also closed with an aluminium plate providing structural support for the injector mount and the optional air heating manifold. The injector sat in a custom designed aluminium mount and was held into place with a brass cap. The fit between those two components was designed to provide enough seal for fuel pressures larger than 150 bar. The high pressure fuel line was connected to the brass cap with compression fittings (Swagelok Company).

The injected fuel was conditioned in a fuel preparation section. A pneumatically actuated pump was supplying fuel from a reservoir to the system at pressures of 150 bar. The fuel pressure was adjusted with a needle valve and controlled via a pressure gauge connected to the fuel line. A pressure cylinder was installed between the pump and the injector to dampen any pressure fluctuations caused by the opening of the injector. A drain valve at the bottom of the section allowed for purging the system and replacing the fuel with a different blend. Also a bleeding and pressure relief valve was installed in order to remove the air from inside the system and relieve the fuel pressure if necessary.

The injector was powered and actuated with an engine control unit ECU, controlled by a custom build triggering unit. The injector was a purpose built single hole model injector producing a spray angle of 20° . The injection duration was set to 1.50 ms by the injector control unit.

The development of the measurement technique and all in-situ measurements were performed on a stainless steel metal plate with a surface roughness of $R_a=60\ \mu\text{m}$ (Blackburns Metal LTD). Comparison experiments were done using a quartz glass plate of the same surface roughness (manufactured by UQG optics). Different R_a values were tested and a roughness of $60\ \mu\text{m}$ was eventually selected for the final technique development steps and the later measurements to have enough headroom for potential large liquid film thicknesses during measurements applying this technique. The individual measurement limits are determined by the R_a values. During the development stages it became apparent that the sensitivity threshold of the technique is at around 30% of the R_a . Liquid films with larger thicknesses cannot be resolved reliably beyond this threshold, for a respective surface roughness.

The development of the measurement technique and the comparison between metal and glass plates were performed with a Pike F-032 CCD camera from Allied Vision Technologies. This 14 bit monochromatic camera had a resolution of 640×480 pixels and provided sufficient resolution, dynamic range and sensitivity to quantify a wide range of film thicknesses. The recording rate was 10 frames per second with an exposure of 5 ms. The images were recorded with Allied Vision's SmartView software and stored as a bitmap series. These recordings were subsequently analysed in Matlab 2013b (MathWorks, Inc).

All time resolved measurements involving sprays in the injection chamber were performed with a high speed CMOS camera of the type HighSpeedStar 6 from LaVision GmbH. The image resolution was 1024×1024 with a digitisation depth of 12 bit. Images were recorded at a frame rate of 2000 fps and an exposure time of 0.5 ms. The camera was mounted with its viewing axis tilted downwards from the horizontal by 10° . A Scheimpflug adapter was set to 20° to improve the depth of field [48]. The injection system was triggered by the high speed controller of the camera, in order to synchronise the recording with the injection. The raw images were captured in Davis 7.2 (LaVision GmbH) and processed in Matlab 2013b using the same basic algorithms as for the images acquired during the methodology development phase.

In all cases a 50 W halogen light source was used which was placed close the camera lens at an angle of about 40° relative to the orientation of the impingement plate and 10° relative to the camera as indicated in Fig. 1 (please note that the light source is not shown in the actual photograph of the experimental setup, but only in the schematic drawing). The illumination cone of the light bulb had an angle of 10° . The bulb was powered by a 12 V DC power supply (IPS1810H, ISO-TECH) to avoid fluctuations in the illumination intensity.

During the development of the methodology, several factors influencing the sensitivity and reliability of the results, were investigated. The angle of the optical setup (light source, camera)

play a significant role. Additionally, the feasibility range of the measurements depend on the surface roughness of the plate, which needs to be selected according to the expected range of film thicknesses. In general, it was found that the light source positioned close to the camera is preferred for this application with the camera at a larger angle. Due to the restricted optical access to the injection chamber, the described optical arrangement was found to be the optimum for these experiments.

3. Development of the liquid film thickness measurement

3.1 Fundamental principle

The basic principle of the technique for the measurement of liquid film thickness is the change of scattering patterns of a roughened surface exposed to liquid deposit of varying thickness. The fundamental mechanism underlying this technique is shown in Fig. 2.

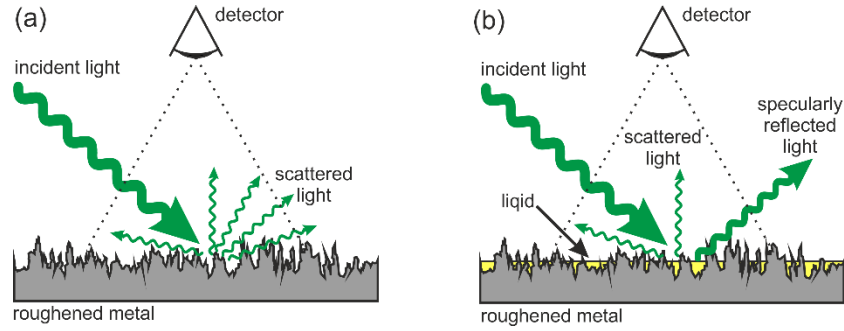


Fig. 2. Optical surface phenomena in case of a roughened metal plate without (a) and with (b) liquid covering the surface.

In case of a homogeneously roughened metal surface incident light illuminating the plate at a defined angle is scattered diffusely in all directions. Part of the light is scattered towards the detector, which is located well outside the specular reflection angle. When a liquid is deposited on the surface a partially smooth surface is created. For this reason the part of the incident light which is reflected specularly increases, while the amount of the light that is scattered towards the detector is reduced. The actual amount of specular reflection depends on the extent of the smooth part of the surface, which increases with the amount of liquid on the plate until the thickness of the liquid layer is larger than the roughness. By carefully selecting the angle of the incident light and the angle of detection relative to the metal plate, it is possible to correlate this intensity change $R(x, y)$ to the actual thickness of the liquid deposit:

$$R(x, y) = 1 - \frac{i_{liq}(x, y)}{i_0(x, y)} \quad (1)$$

with

$$i_0(x, y), i_{liq}(x, y) = f(d(x, y)) \quad (2)$$

where i_0 is the local intensity without any liquid present, i_{liq} the respective intensity with a liquid film covering the surface, d the thickness of the film and x and y are the local coordinates. Note that the function $f(d(x, y))$ is nonlinear and that it is based on a calibration which is only valid if the optical setup is kept unchanged.

In order to verify these assumptions, tests were performed comparing the metal surface to a glass surface at ambient temperature, following the approach of the Refractive Index Matching

method presented by Drake *et al.* [38]. For this purpose, both the metal and the glass plates were installed and tested in the fuel injection chamber. The angles of the light source and the camera were kept the same in each case. The fuel injection was triggered by the initiation of recording by the camera, making sure to record the entire process, which included the surface before and after impingement. Please note that it is not possible to record reliable data during the actual injection process, because the spray is blocking the direct line of sight of the liquid film.

From the recorded images, the average normalised intensity i_{liq}/i_0 was calculated for an area of $5 \times 5 \text{ mm}^2$ at the centre of the liquid film. The selected area of each frame was divided by the same area of the reference frame without a liquid. The results for both plates are presented in Fig. 3.

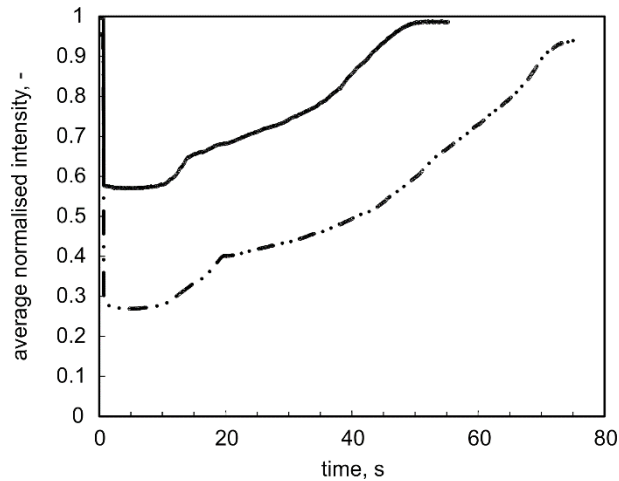


Fig. 3. Comparison of the area averaged normalised intensity of a roughened metal (—) and a roughened glass plate (---).

The overall shape of both curves looks very similar, only the sensitivity (i.e. the change of the scattered light intensity) is different. Before the fuel injection, the normalised intensity equals one. The impingement of the spray results in the formation of a liquid deposit and, as such, causes a sudden decrease of the normalised intensity. Over time, as the liquid deposit evaporates, the intensity gradually increases again. It should be noted that the images were not corrected for noise, which is why the values do not become unity again. Both plots are comprised of segments with different slopes. In general, the evaporation process is significantly quicker with the metal plate, probably caused by the larger thermal conductivity of the metal. In comparison to the glass plate, the metal plate shows a smaller sensitivity. The smallest value of the normalised intensity for the metal plate in this test is approximately twice as large as that for the glass plate (appr. 0.6 for metal and 0.3 for glass). A possible explanation could be that for the non-transparent metal plate, the effect of refracted light is missing. This means that the incident light always gets reflected and scattered completely. Despite this difference, the results provide good evidence that, with an appropriate calibration, it is possible to correlate the intensity change to the actual film thickness of the deposit, as both cases are able to portray the multi-phased evaporation behaviour of the liquid.

3.2 Calibration method and data processing

In order to calibrate the optical setup, known volumes of liquid were applied to a well-defined area on the metal surface, while recording images with the CCD camera. Due to capillary forces generated by the surface asperities, the liquid spreads immediately after getting in contact with the surface [39]. Dodecane was chosen as a calibration liquid, because of its low volatility. Furthermore, its wettability on metal surfaces proved to be very good. Using this liquid, it was

possible to generate very thin films while minimising systematic errors caused by evaporation. In order to verify this, 1 μl of dodecane was dropped on a rough metal plate, which was placed on a micro balance (R200D, Sartorius Research) at room temperature. Over the course of 10 minutes the change in mass was less than 0.5%. Based on this, the amount of dodecane was considered to be stable for the duration of each calibration point. The liquid was applied to the surface with the help of a microliter pipette (Rainin Classic PR2 0.1-2 μL , Anachem Ltd). In order to define the area of the metal plate that the liquid can cover, a circular paraffin boundary, approximately 15 mm in diameter, was created with a PAP pen (Marker PAP PEN Immunostaining, VWR). As such, it was possible to not only generate very thin films, but also create homogeneous thicknesses significantly larger than 10 μm . An important advantage of the technique is that the calibration is independent of the liquid that is used, as long as the reflective index has the same magnitude and the wetting behaviour is similar. Therefore, the calibration with dodecane is valid for all liquids with a similar refractive index, which is the case for the fuels investigated here.

In order to obtain a calibration function based on Eq. (1), known volumes of dodecane were deposited on the roughened metal plate while recording images. The recorded images at the beginning with no liquid on the surface were used to calculate the initial intensity i_0 . Once the liquid film was spread evenly across the surface, series of images were obtained from which the intensity i_{liq} could be calculated. By repeating these steps with different amounts of liquid, it was possible to derive the relation between liquid film thickness d and the change of intensity ratio R . After recording the images with the CCD camera, several processing steps were performed. These are shown in Fig. 4. Both the reference image [Fig. 4(a)] and the image with the liquid film [Fig. 4(b)] were corrected for optical distortion using the dewarping feature provided by Davis software [results in Fig. 4(c) and Fig. 4(d)]. In this way, it was also possible to determine the magnification scale of the pixels. The two dewarped images essentially correspond to i_0 and i_{liq} . Therefore, it was possible to calculate a two-dimensional intensity ratio based on Eq. (1), when dividing the two images by one another and subtracting the result from the value one. This step yielded Fig. 4(e), where the region, which was not covered by the liquid, had a value of approximately zero and appears black and a region covered by the liquid with values between one and zero, corresponding to a certain film thickness. The next set of processing steps had the aim to detect the area that is covered by the liquid. In order to increase the contrast ratio between these two areas a non-linear diffusion filter (NLD) was applied, following the guidelines from Weickert *et al.* [49, 50] and also a 3x3 median filter [Fig. 4(f)] to reduce the noise. The result can be seen in Fig. 4(g) where the area covered by liquid shows very high intensities while maintaining the initial boundary between liquid and non-liquid. As a last step, a binarisation algorithm was applied [51]. A threshold was determined based on an intensity analysis of the image. Pixels with values larger than this threshold become one, pixels with smaller values are set to zero. The algorithm also used a clean-up routine to remove the small black islands created in the previous steps. With the information contained in picture Fig. 4(h), the boundary of the liquid film could be calculated. Using this data, an area averaged intensity ratio could be derived from Fig. 4(c). Knowing the volume that was deposited on the metal plate, the calculated intensity ratio could be linked to an area averaged liquid film thickness. By repeating the entire process with different volumes, a correlation between film thicknesses and intensity ratios could be generated. Fig. 5 presents an example of such a calibration function.

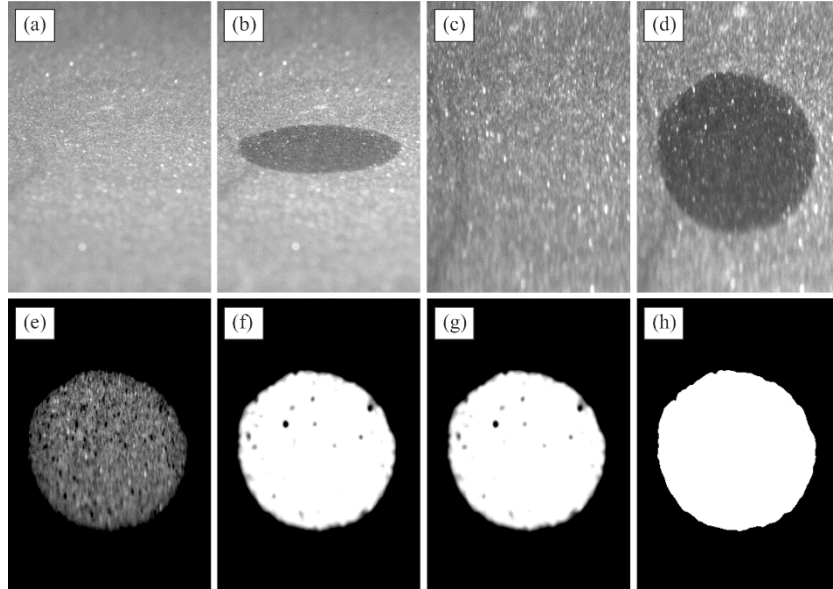


Fig. 4. Image processing to derive the calibration function

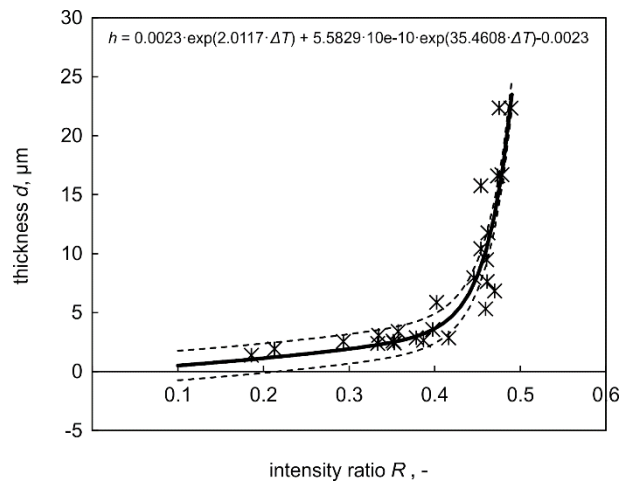


Fig. 5. Calibration points (×) obtained during the calibration procedure are shown with a double exponential fit (—), error approximation (---) and the calibration function.

In this case, the calibration function was derived from a least squares fit method using a double exponential function in the form of

$$y = a \cdot e^{bx} + c \cdot e^{dx} + e \quad (3)$$

The dashed lines indicate an uncertainty of 1.25 μm in film thickness, which corresponds to a volume of approximately 0.2 μl (10% of the pipette maximum) of liquid. With this approximation it can be seen that the sensitivity of the method varies notably with the thickness of the liquid film. Basically, the plot can be split into two regions. Between zero and about 0.4 intensity ratio there is a high sensitivity towards changes in the film thickness. For intensity ratio values larger than 0.5 the calibration becomes very insensitive, which is why thicknesses larger than 0.25 mm cannot be captured reliably with this setup. A change in the optical

arrangement or a different roughened metal plate would be necessary to further extend the measurement range towards larger values.

The data processing used for analyzing the measurements follows similar image processing steps as the calibration. Using the dewarped images before [Fig. 6(a)] and after [Fig. 6(b)] the liquid impingement on the surface, the intensity ratio was calculated. By applying the calibration function, the actual two-dimensional film thickness could be calculated as shown in Fig. 6(d). Essentially, this process yields the quasi-instantaneous two-dimensional information of the liquid film thickness, from which the cumulative deposit volume can also be calculated. If these steps are repeated for all the recorded high speed images, one can calculate the total volume of the liquid film over time.

Please note that this is a line of sight measurement technique. Because of this it is not possible to reliably detect the liquid film during the impingement as the spray impedes direct view of the liquid film. Once the injection is complete and the spray itself is gone reliable data of the wall deposit can be obtained.

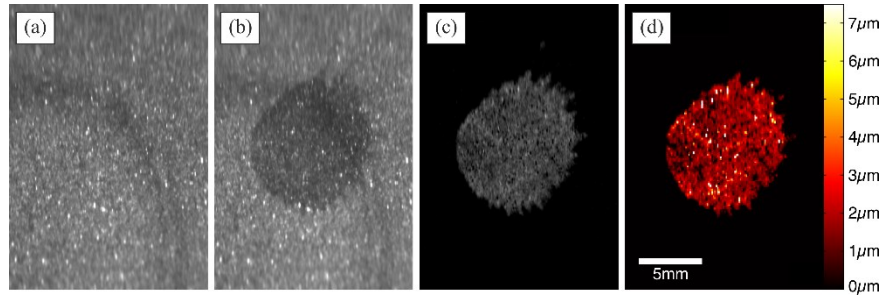


Fig. 6. Image processing used to analyse liquid films: dewarped images before (a) and after (b) the impingement, the calculated intensity ratio (c) and the actual film thickness after applying the calibration function (d).

4. Measurement uncertainty

The optical alignment angles of the camera and the light source relative to the impingement plate play a significant factor for the measurement technique. During the development of the technique it was found that a shallow angle leads to an oversensitive setup, where even very thin liquid films already lead to intensity ratios larger than 0.5. This also makes the technique very insensitive towards changes of thicker liquid films. At the other end of the spectrum are angles that cause direct reflections of the light source towards the camera. These need to be avoided completely. This issue might not be evident without a liquid film on the rough surface because the incident light gets scattered evenly and the surface appears grey. Once a deposit is partially smoothing the rough surface, regions of very high intensity are recorded. The intensity values associated with these areas are larger than those without a liquid which would result in a negative intensity ratio and makes the measurement invalid. The angles that were chosen for the present experimental setup were mainly determined by the compromise between sensitivity, measurement range and optical access of the setup. By using a different light source and recording optics (e.g. endoscope or fibre optics) it would be possible to extend the range of the alignment angles and thus broaden the applicability of the setup, especially in optical engines with limited access.

Other factors that contribute to measurement uncertainty can be split into two categories, errors that affect the calibration procedure and errors that occur during measurements. When calibrating the setup, the largest uncertainty comes from applying defined volumes of liquid on the plate with the microliter pipette. As shown in the calibration plot [cf. Fig. 4.3] for the used setup the intensity ratio is quite sensitive towards errors in the transferred volume of the liquid in the region between 0.1 and 0.4. For intensity ratios that are larger than 0.4, the error

approximation is converging with the calibration line as the relationship becomes more insensitive with changes in the film thickness. The approximation of a constant error of $0.2 \mu\text{l}$ as shown in Fig. 5 was used to illustrate the two sensitivity regions of the calibration and is overestimating the error for smaller volumes that were applied to generate calibration thicknesses. An error of 10% relative to the actually applied liquid volume results in approximately 10% error of the film thickness for a given area. With that the intensity ratio is fluctuating by approximately ± 0.03 in this range.

The image processing steps necessary to detect the boundaries of the liquid film and to determine the film area can induce a minor shift of the film front by two pixels in the worst case. The intensity gradient based binarisation algorithm cannot produce sub-pixel accuracy of the boundary, but is limited to a whole pixel. Effectively, this corresponds to an offset of plus or minus one pixel. For this worst case approximation of a two pixel shift and a given magnification of the setup this results in a length of 0.116 mm. In relation to the circular area with a diameter of approximately 15 mm that was used during the calibration (created with the paraffin pen) this equates to an error of less than 1.6% relative to the film area. Because of the small magnitude, the accuracy of the boundary detection procedure of the liquid film is satisfying and this error will not be considered in the discussion of the results obtained with this method.

Noise introduced by the DC power supply will also be neglected for the discussion. The power supply was specified for fluctuations of 1 mVrms at 12 V operating voltage. The cameras were left to warm up for at least 30 minutes until a stable operating temperature of the internal cooling system was achieved. In this way, the drift in the sensitivity of the chips during measurement was minimized. In addition, the noise calibration feature provided in the recording software was used to subtract the noise of the dark image, before each measurement. With this, the noise generated by the recording electronics was minimized and kept constant for all experiments.

During measurements the main uncertainty was introduced through fluctuations from injection to injection. It was observed, that the values of the maximum deposit volume measured could fluctuate by up to $\pm 10\%$. To ensure reasonable significance of the data, measurements were repeated five times and the mean value as well as the standard deviation were calculated.

5. Results

This study focussed on developing an optical technique, which can be used to investigate the fuel spray-piston interactions that occur inside a gasoline direct injection engine. In order to demonstrate the potential application of this technique, a selection of single component fuels with known physical properties were tested in the fuel injection chamber. The fuels were selected so that the effects of the boiling temperature of the liquid on the measured liquid deposit and its evaporation time can be considered.

The first set of single component fuels consisted of the linear alkanes hexane, heptane and octane (all technical grade, VWR International). The properties of these chemicals are very well investigated and share some similarities with the components found in regular gasoline. The three chemicals have comparable thermo-physical properties with virtually the same density, heat capacity and heat of evaporation. The viscosity and surface tension change by small amounts. The second set of fuels comprised of ethanol, propanol and butanol (technical grade, VWR International), representing linear alcohols. Unlike the alkanes, these chemicals have different thermo-physical properties regarding viscosity, heat capacity and heat of evaporation. Only the density and surface tension do not change significantly. A summary of the physical properties can be found in Table 1.

Table 1. Physical properties of the liquids investigated [52].

fuel	boiling temperature, °C	density, g/cm ³	viscosity, mPas	surface tension, dyn/cm	heat capacity, J/(K kg)	heat of evaporation kJ/kg
hexane	69	0.659	0.326	18.40	2293.69	334.78
heptane	98	0.684	0.386	20.14	2241.87	364.26
octane	126	0.703	0.542	21.62	2238.32	362.01
ethanol	78	0.789	1.144	22.39	2420.96	837.02
propanol	97	0.803	1.938	23.79	2406.19	689.57
butanol	117	0.810	2.544	24.20	2386.08	584.04

In the case of the alkanes only the boiling temperature varies significantly. In this way, potential differences in the liquid film thickness can be linked mainly to the boiling temperature of the liquids.

In the first set of experiments the plate temperature was maintained constant at 100 °C for all fuels (alkanes and alcohols). The injection duration was kept constant at 1.50 ms and the air temperature inside the test chamber was constant and only affected by the plate temperature (steady state). From the recorded high speed images, the cumulative volume of the liquid deposit was measured as a function of time using the approach and the calibration that were described in the previous section. These measurements are presented in Fig. 7 and Fig. 8 with time starting when the injector is triggered.

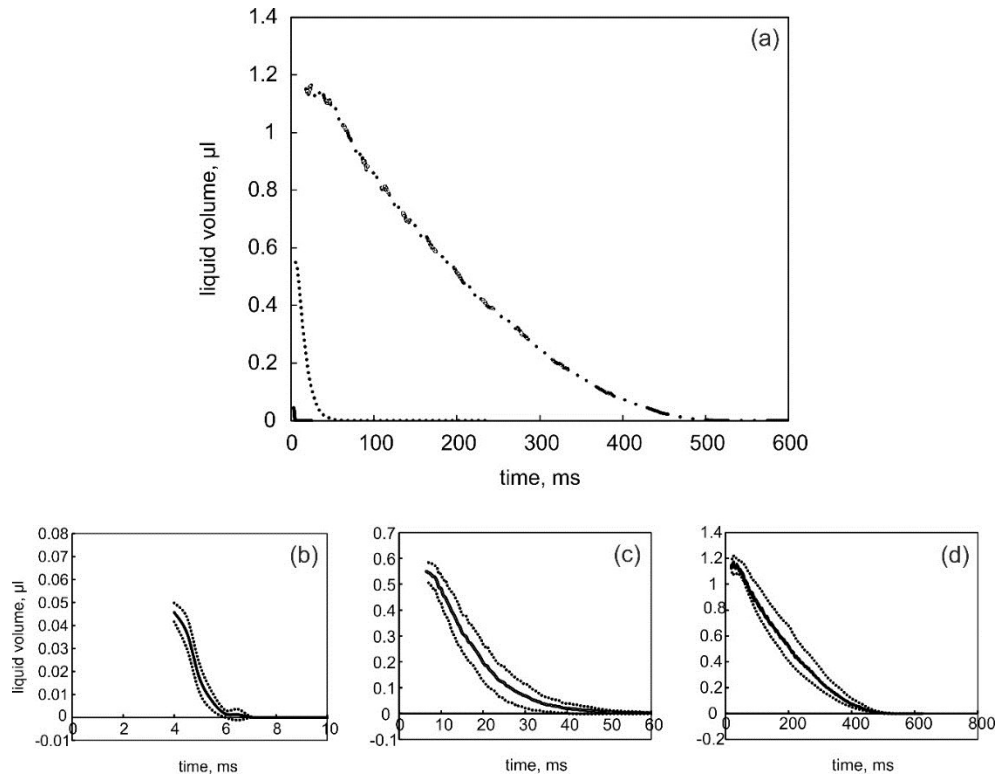


Fig. 7. Mean liquid volume of wall deposit of hexane (—), heptane (....) and octane (-.-) fuels as a function of time after triggering the injector and a plate temperature of 100°C (a) and the individual mean time signal (—) for hexane (b), heptane (c) and octane (d) including the respective standard deviation (....).

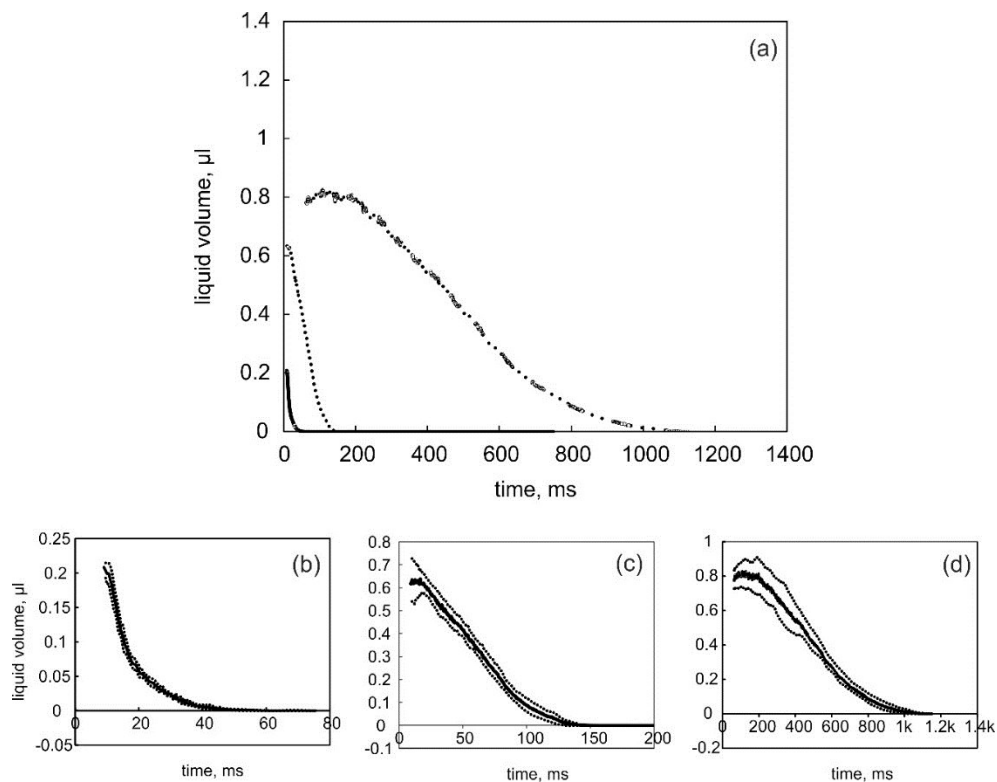


Fig. 8. Mean liquid volume of wall deposit of hexane (—), heptane (····) and octane (—·—) fuels as a function of time after triggering the injector and a plate temperature of 100°C (a) and the individual mean time signal (—) for hexane (b), heptane (c) and octane (d) including the respective standard deviation (····).

With increasing boiling temperature of the alkanes, the volume of the liquid deposit increases significantly. Hexane produces almost no liquid film compared to the other two fuels. The film generated by octane has about twice the thickness of heptane and takes an order of magnitude longer to evaporate. The behaviour of the three alkanes indicates the significance of the boiling temperature and the surface temperature if it comes to formation of liquid deposits post injection. Having a plate temperature higher than the boiling temperature leads to almost no deposit in case of hexane, while having a plate temperature lower than the boiling temperature produces very large deposits in the case of octane. Looking at the individual plots of the liquid deposit volume [Figs. 7(b), (c) and (d)] it can be seen that the standard deviation shows a similar characteristic for the alkanes. Only in the case of hexane do the fluctuations between the recordings seem to be less pronounced. Overall it can also be seen that the standard deviation becomes smaller as the liquid film evaporates completely and converges with the mean value.

Similar observations can also be identified with the linear alcohols. Looking solely at the boiling temperature, the order of the liquid fuel thickness follows the same sequence as for the alkanes. It should be noted that with all alcohols, but more significantly for propanol and butanol, boiling was observed inside the film. This was not observed with the alkanes. This is the reason that the measured liquid volume at the early stages of spray impingement for alcohols in Fig. 8 is lower than the volume for alkanes in Fig. 7. The formation of bubbles inside the liquid film alters the scattering behaviour of the incident light and also modifies the evaporation rate of the liquids. The larger the deposit, the more pronounced the bubble formation inside the liquid. Despite this different behaviour, it appears that if the boiling temperature is lower than the plate temperature the deposit is small, and the opposite if the boiling temperature is higher. Essentially, the same liquid film behaviour is observed with the alcohols as with the alkanes.

The separate plots of each alcohol [Figs. 8(b), (c) and (d)] show that the standard deviation increases from ethanol to propanol and butanol. Fluctuations between the ethanol injections are very small and the standard deviation follows the mean value very closely. The other two fuels have more variances between injections, especially at the beginning of the recording in the region close to the initial deposit volume. Over time, the standard deviation lines are also converging with the mean, similar to the alkanes

Comparing the results of the alkanes in Fig. 7 with the alcohols in Fig. 8, it is noticeable that the time scale of evaporation of the liquid film is significantly longer for the latter, almost around two times. Looking at the physical properties, the larger heat of evaporation of the three alcohols is apparent. However, the fuel with the smallest heat of evaporation of the alcohols, butanol, takes the longest to evaporate. This could mean that the different behaviour alcohols vs. alkanes might not only be connected to this property.

To further elaborate on this matter the total energy to evaporate the fuel film, based on the physical properties shown in Table 1, was calculated. Table 2 shows these values. The theoretical deposit volume, which was used to estimate the total evaporation energy required for each fuel, assumes that the entire volume of spray gets deposited during injection. This assumption neglects any real interaction between the spray and the surface, and can be regarded as a worst case scenario. The resulting film volume is 15 μl , based on the flow rate information provided by the manufacturer of the injector. Based on this deposit volume, the energy required to heat up each liquid to boiling temperature can be calculated, assuming that the initial film has a temperature of 20 °C. Once the film reaches boiling temperature, the energy to evaporate the liquid was calculated using the latent heat of evaporation from Table 1. By combining these two values, the theoretical total energy was calculated.

Within the group of alkanes the total energy based on this theoretical deposit volume increases as the boiling temperature becomes larger. The reason for this is that the latent heat of evaporation is almost identical between the three fuels. Therefore, the only contributing factor is the boiling temperature and the energy required to heat up the liquid. Ultimately, this yields a trend which agrees with the results found in the experiments.

In case of the alcohols, however, this trend cannot be observed. Similar to the alkanes, the energy required to reach boiling temperature increases from ethanol to butanol. Albeit, the latent heat of evaporation decreases significantly at the same time. So much in fact, that the energy required to evaporate the respective alcohol compensates for the increasing energy required to reach boiling temperature of the fuels. In the end, the total energy necessary to evaporate each alcohol does not increase with the boiling temperature.

If the total evaporation energy is calculated in the same way as before, but based on the maximum volume measured in the experiments, one can see the same trend as observed in the experiments. With increasing boiling temperature of the single component fuel, the total energy to evaporate the deposit also increases. Furthermore, if the alkane is compared to the alcohol with a similar boiling temperature, one can see that the required energy is higher. This could explain why the initial deposit volume is higher in case of the alcohols, again with the exception of butanol.

Table 2. Calculated evaporation energy for each fuel based on a theoretical deposit volume and on the measured volume.

fuel	energy to reach boiling temperature, J	energy to evaporate, J	total energy based on the theoretical volume, J	total energy based on the measured volume, J
hexane	1.11	3.31	4.42	0.13
heptane	1.79	3.74	5.53	0.20
octane	2.50	3.82	6.32	0.49
ethanol	1.66	9.91	11.57	0.16
propanol	2.23	8.31	10.54	0.44
butanol	2.81	7.10	9.91	0.54

In order to further understand the significance of the surface temperature on the liquid deposit formation and evaporation, a second set of experiments was conducted. This time, the surface temperature was adjusted during each measurement to match the individual boiling temperature of the liquid. The measurements were analysed in the same way as before and are presented in Fig. 9 and Fig. 10.

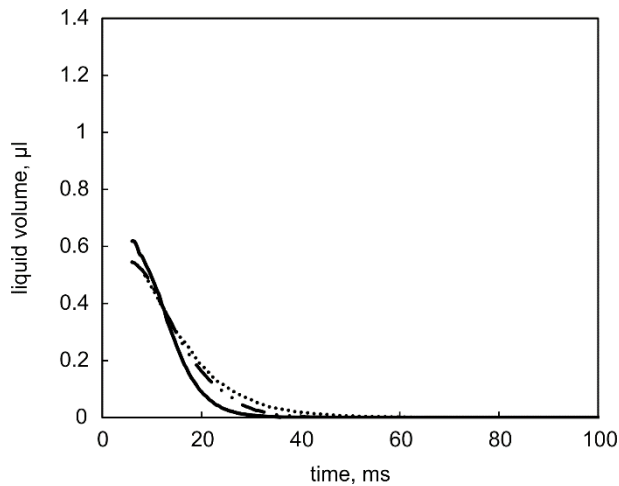


Fig. 9. Liquid volume of wall deposit of hexane (—), heptane (.....) and octane (---) fuels as a function of time after triggering the injector and with the plate temperature matching the boiling temperature of each individual liquid.

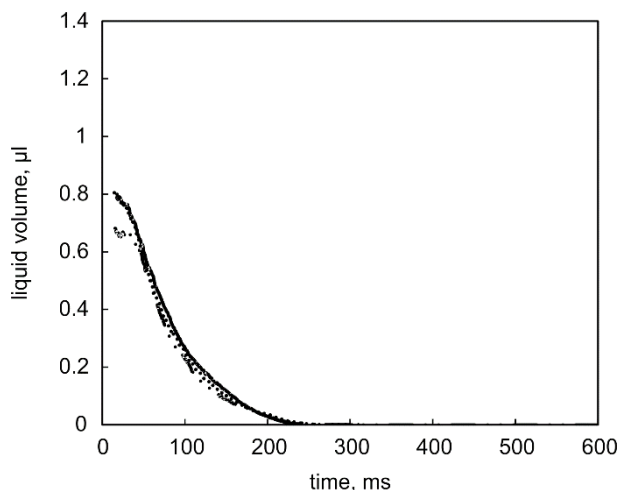


Fig. 10. Liquid volume of wall deposit of ethanol (—), propanol (....) and butanol (-.-) fuels as a function of time after triggering the injector and with the plate temperature matching the boiling temperature of each individual liquid.

The results show that the curves of evaporation of the liquid film as a function of time for each set of liquids now overlap nearly perfectly. As mentioned before, in the case of the alkanes, the only physical property that varies significantly is the boiling temperature. This means that adjusting the plate temperature to match the boiling temperature of the liquid has a dramatic impact on deposit formation and evaporation. Surprisingly, the three alcohols seem to behave in the same way, despite them having less similarities in their physical properties than the alkanes. This would mean that the boiling temperature of the liquid is the most influential property for the liquid deposit formation and evaporation, which is remarkable.

Between the two families of fuels, a difference in the time scale remains with the alcohols taking 5-6 times as long as the alkanes to evaporate, although the initially deposited volume is similar. Please note, that all alcohols also showed minor boiling inside the film, similar to the first set of experiments, which was most pronounced in the case of butanol. This could explain that the initial deposit volume of butanol appears to be smaller compared to ethanol and propanol. Similar to the 100 °C case, the scattering behaviour could be affected by bubble formation, which reflects more light towards the camera, and therefore results in a calculated film thickness smaller than the actual value.

Overall, the results show the significance and importance of the relationship between the surface temperature and the boiling temperature of the liquid. If this observation is applied to the cylinder wall and piston wetting inside a direct injection engine, this would mean that by increasing the wall and piston surface temperature inside an engine to match or exceed the boiling temperature of the fuel, the amount of liquid deposit will be reduced significantly. This finding has the potential to reduce the amount of particulate emissions from modern gasoline engines, since the exhaust particulate emissions are linked to the liquid film formation during the injection process 1.

6. Summary and Conclusions

A novel method to investigate the physics of liquid fuel deposits and evaporation, created by a spray of a fuel injector impinging on a piston or wall surface, was developed. The technique makes use of the change of the liquid scattering intensity emitted from a metal surface with known roughness, when liquid is deposited. Important advantages of the technique over previously established methods are the ability to measure time-dependent spatial distribution of liquid film thickness without a need to add a fluorescent tracer in the liquid, while the measurement principle is not influenced by changes at the pressure and temperature of the liquid

or the surrounding gas and liquid properties. However, an *in-situ* calibration of the dependence of signal intensity on liquid film thickness is required for each optical setup. Therefore, the developed method can be applied to measure the time-dependent and two-dimensional distribution of the liquid film within the environment of gasoline direct injection engines. However, the technique can also be applied to numerous applications, where liquid film deposits on a solid non-transparent surface is important. The main findings of the paper are presented below.

- The principle of the technique, the data processing approach and the calibration procedure were presented and demonstrated. A comparison of the evaporation behaviour of liquid fuel deposited on a metal and a glass plate was also performed, to further demonstrate the applicability of the technique.
- The application of the technique was demonstrated by selecting linear alkanes and alcohols with changing boiling temperature and studying the behaviour of the liquid film thickness on a metal impingement plate with variable temperatures. When keeping the surface temperature constant at 100 °C, an increase in the liquid film thickness was observed with increasing boiling temperature, both with the alkanes and the alcohols. By adjusting the plate temperature from 100 °C to match the boiling temperature of each individual fuel, it was possible to overlap the evaporation curve of all alkanes and alcohols respectively. This means that not only the time scale until complete evaporation was similar within each group of fuels, but also the initial volume of the liquid film. Overall, this shows the strong influence of the boiling temperature of the fuel on the behaviour of the liquid film thickness, which suggests that control of the wall temperature in the cylinder of a gasoline direct injection engine may reduce the liquid fuel deposit, which may assist the reduction of particulate emissions at the exhaust.
- Future work is required to further develop the technique and make it more independent towards the effects of the angle of illumination and detection. This would broaden the applicability and open it up for numerous investigations.
- The necessity of an *in-situ* calibration might prove obstructive for the transfer of the technique to metal test engine. By further understanding the effect of the light source and optics positioning it could be possible to abstract this step outside of the actual chamber and apply it inside the cylinder during later measurements. In combination with endoscopic optical access this would make the technique viable in real engines.
- Finally, the effect of surface roughness on the evaporation rate of thin liquid films should be evaluated, which may assist the reduction of wall wetting in IC engines.

Acknowledgments

The authors gratefully acknowledge financial support from Shell Global Solutions for parts of this work.